COMMUNICATION

New Route to Battery Grade $NaPF_6$ for Na-Ion Batteries: Expanding the Accessible Concentration

Darren M. C. Ould,[a,b] Svetlana Menkin,[a,b] Christopher A. O'Keefe,[a,b] Fazlil Coowar,[c] Jerry Barker,[c] Clare P. Grey*[a,b] and Dominic S. Wright*[a,b]

[a] Dr. D. M. C. Ould, Dr. S. Menkin, Dr. C. A. O'Keefe, Prof. C. P. Grey and Prof. D. S. Wright
Yusuf Hamied Department of Chemistry
University of Cambridge, Lensfield Road, Cambridge, CB2 1EW, U.K.
E-mail: cpg27@cam.ac.uk dsw1000@cam.ac.uk
[b] Dr. D. M. C. Ould, Dr. S. Menkin, Dr. C. A. O'Keefe, Prof. C. P. Grey and Prof. D. S. Wright
The Faraday Institution, Quad One, Harwell Science and Innovation Campus, Didcot, U.K.
[c] Dr. F. Coowar and Dr. J. Barker
Faradion Limited, The Innovation Centre, 217 Portobello, Sheffield, S1 4DP, U.K.

Supporting information for this article is given via a link at the end of the document.

Abstract: Sodium-ion batteries represent a promising alternative to lithium-ion systems. However, the rapid growth of sodium-ion battery technology requires a sustainable and scalable synthetic route to high-grade sodium hexafluorophosphate. This work demonstrates a new multi-gram scale synthesis of $NaPF_6$ in which the reaction of ammonium hexafluorophosphate with sodium metal in THF solvent generates the electrolyte salt with the absence of the impurities that are common in commercial material. The high purity of the electrolyte (absence of insoluble NaF) allows for concentrations up to 3 M to be obtained accurately in binary carbonate battery solvent. Electrochemical characterization shows that the degradation dynamics of sodium metal–electrolyte interface are different for more concentrated (>2 M) electrolytes, suggesting that the higher concentration regime (above the conventional 1 M concentration) may be beneficial to battery performance.

The ever-growing demand for electrical energy production and large-scale grid storage has led to a surge in research efforts in recent years into sodium-ion batteries (SIBs).[1–5] Although the lithium-ion battery (LIB) field currently dominates and is well established, arguably one of the most attractive features of moving towards SIBs is the significantly higher abundance of sodium compared to lithium. Moreover, these sodium deposits are evenly distributed worldwide so are less susceptible to geopolitical price fluctuations and are much cheaper than lithium.[6] Although the inherently lower energy density has previously plagued SIBs, for large-scale or stationary storage applications this is less of a critical consideration as here, the low cell cost dominates. Given the low abundance and relatively high cost of lithium, it is envisioned that the development of SIBs for grid storage will be critical to relieve the pressure on LIBs, as the surging rise of portable electronic devices and electric powered vehicles is likely to place an insurmountable burden on lithium supplies.[7] Furthermore, the use of sodium has other sustainability implications, which are particularly important for grid-scale applications, as it allows cobalt-free cathodes to be used and the copper current collectors at the anode to be replaced by aluminium.

As sodium sits below lithium in Group 1 of the periodic table, knowledge of the LIB field can help accelerate research and development of SIBs as the general principles are the same for both batteries. This is true in particular of the electrolyte, which plays a crucial role for the overall lifetime, rate capability and safety of the battery, for which direct sodium analogues of lithium electrolytes are normally used.[8–12] From the selection of sodium salts currently available, the present benchmark is sodium hexafluorophosphate, although optimum solvents and concentrations are still widely debated.[13] Organic carbonate-based solvents are typically preferred, in part due to their high dielectric constant and low viscosity, which aids solubility and gives high ionic mobility. Recent work by Younesi and colleagues has shown that ethylene carbonate: diethyl carbonate (EC:DEC) may be advantageous as a solvent due to aiding a more stable solid-electrolyte interphase (SEI), whereas propylene carbonate (PC) leads to a less stable SEI due to the higher solubility of SEI components, such as NaF and Na_2CO_3.[14]

Figure 1. Top: Previous synthetic methods of producing $NaPF_6$. Bottom: This work using ammonium hexafluorophosphate and sodium metal.

Sodium hexafluorophosphate has a number of attractive features as a salt compared to the other commonly used sodium salts. Nevertheless, studies have shown that $NaPF_6$ is highly hydroscopic and readily undergoes hydrolysis to produce NaF, HF and other phosphate species (such as POF_3).[15,16]

Remarkably, this hydrolysis can still take place in battery-grade electrolytes which have <20 ppm of water present,[15] highlighting the highly hydroscopic nature of $NaPF_6$. Consequently, this means that the quality of commercially purchased $NaPF_6$ may be variable and depends on the degree of hydrolysis that has occurred (either through storage or as a result of the synthetic route used to make it). The presence of impurities has a detrimental effect on use in battery research, as these highly insoluble hydrolysis products crucially affects the real electrolyte concentration. Bhide and Adelhelm in recent work reported that when using a high purity (99%) supply of $NaPF_6$, an insoluble fraction appeared beyond 0.4 M concentration when dissolving in ethylene carbonate: dimethyl carbonate (EC:DMC 30:70 wt%). Subsequent X-ray diffraction of the mixture found evidence of NaF (which is also an important solid electrolyte interphase (SEI) component) as the insoluble impurity.[17] Resolving this solubility issue of $NaPF_6$ is therefore of primary importance for the SIB field as fundamental properties of the electrolyte are dependent upon the ions concentration.[13,17]

As commercially purchased $NaPF_6$ may contain insoluble impurities, it would be desirable to synthesize it under anhydrous conditions and immediately use it, thus preventing NaF formation. However, the literature contains few methods to do this and most involve using HF, which has significant safety concerns. One reported synthesis by Woyski is the fluorination of a mixture of sodium and PCl_5 with liquid HF,[18] whereas Clifford's synthesis involves the formation of PF_5 from red phosphorus, HF and ClF_3 and subsequent reaction with NaF.[19] A patented method from South Africa Nuclear Energy involves the reaction of pyridinium hexafluorophosphate, synthesized from HF, phosphoric acid and pyridine, with sodium hydroxide,[20] whereas Astruc has shown $NaPF_6$ may be produced from reduction of CpFe(II)(arene) hexafluorophosphate with sodium amalgam at −20 °C (Figure 1).[21] Clearly these synthetic routes all contain a number of hazardous or expensive steps that make the synthesis of $NaPF_6$ inaccessible without special control measures and specialized equipment. Alternatively, electrolyte solutions of $NaPF_6$ in carbonate solvent may be commercially purchased, but their high cost can be prohibitive.

Similar synthesis routes exist for producing $LiPF_6$,[22,23] where early methods involved the addition of LiF to PF_5 in anhydrous HF.[24] This protocol may be used in acetonitrile solvent, but gives a tetra-coordinated solvated lithium cation.[25] The solvated $Li(CH_3CN)_4PF_6$ salt can also be produced from the reaction of HPF_6 with LiOH.[23] Alternatively, unsolvated $LiPF_6$ may be synthesized from direct fluorination from LiF and phosphorus in a fluorine atmosphere.[26]

Herein, we address the urgent need to produce high grade $NaPF_6$ that is suitable to act as an electrolyte salt, showcasing a simple and inexpensive method using ammonium hexafluorophosphate and metallic sodium. This method does not involve the use of HF or aqueous conditions and can be readily performed in a laboratory setting without specialist or expensive equipment.

Previously our group has reported that magnesium hexafluorophosphate can be synthesized from nitrosonium hexafluorophosphate ($NOPF_6$) with magnesium turnings in acetonitrile solvent.[27] However, this synthetic route is inappropriate for producing $NaPF_6$ as sodium metal reacts with acetonitrile and other solvents were found to react with $NOPF_6$. In search of a new protocol, ammonium hexafluorophosphate (NH_4PF_6) was instead employed, which has the additional benefit of reduced cost compared to $NOPF_6$ (see SI for cost analysis of synthesized $NaPF_6$).[28]

$NaPF_6$ was synthesized by firstly dissolving NH_4PF_6 in THF solvent. Once dissolved, this was added dropwise to freshly cut metallic sodium suspended in THF, which immediately gave effervescence due to the release of dihydrogen and ammonia gas as the only by-products. The reaction was heated to reflux for six hours, then left to stir for a further sixteen hours at 50 °C, which after removing the excess sodium by filtration and drying under vacuum produced $NaPF_6$ in an excellent yield of 89% (Scheme 1). Two equivalents of sodium metal were found to be optimal for the synthesis as using stoichiometric or a small excess (1.2 equivalents) failed to consistently give complete conversion using the above stated conditions. Furthermore, the scalability of this protocol has been shown by producing 24 g of $NaPF_6$ (See SI).

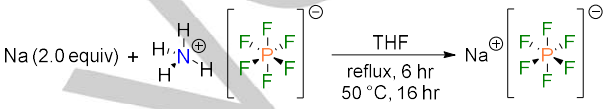

Scheme 1. Synthesis of sodium hexafluorophosphate from metallic sodium and ammonium hexafluorophosphate.

Initial characterization of the $NaPF_6$ salt was performed using solution-state NMR spectroscopy (Figures S2.1.1–S2.1.3). Analysis of both the ^{31}P NMR and ^{19}F NMR spectra revealed the expected septet and doublet signals at −144.6 ppm and −73.2 ppm respectively, confirming the presence of the PF_6^- anion. More informative was the ^1H NMR spectrum, which showed the absence of an ammonium signal, which appears at *ca*. 5.9 ppm. Furthermore, on account of the strong donor ability of the THF solvent, the ^1H NMR spectrum showed residual THF solvent signals at 3.64 ppm and 1.79 ppm, despite drying under vacuum for 16 hours. The addition of 1,4-dimethoxybenzene as an internal standard showed these THF signals account for *ca*. 3% of the sample (Figure S2.1.4).

Attempts were made to fully remove the residual solvent by drying under vacuum at both ambient temperature and at 160 °C for 72 hours and 24 hours respectively, but both cases still showed THF solvent signals in the solution-state ^1H NMR spectrum. However, precipitating $NaPF_6$ from a concentrated solution of THF with pentane and drying under vacuum at 120 °C for 24 hours was found to reduce the intensity of the THF signals, albeit not fully removing them (see SI and Figure S2.1.7).

Additionally, the scope of this synthetic procedure was also investigated by synthesizing KPF_6. This proceeded in analogous fashion to the $NaPF_6$ synthesis, with the addition of NH_4PF_6 to metallic potassium in THF solvent; solution-state NMR spectroscopy again confirmed the presence of the PF_6^- anion and loss of NH_4PF_6 starting material (SI and Figures S2.1.8–S2.1.10).

With $NaPF_6$ in hand, solid-state NMR (SSNMR) spectroscopy was used to assess the purity of the salt as it allows the identification of insoluble chemical species, even if they are present at low concentrations (Figure 2). Figure 2a shows the ^1H solid-state NMR spectrum, which consists of several signals with low signal-to-noise ratios, suggesting a low concentration of proton-containing species. These signals are assigned to the minor amount of THF that is incorporated into the material, with the appearance of several peaks being a result of crystallographically distinct protons in the THF molecules. The ^{19}F

spectrum has a doublet centered at –81.1 ppm with overlapping, low-intensity multiplets underneath (Figure 2b). The additional signals are likely due to minor amounts of hydrolysis product impurities (e.g., $PO_2F_2^{2-}$, POF_3^-); however, the overlap with the $NaPF_6$ signal precludes quantification of these impurities using ^{19}F NMR spectroscopy. On the other hand, in the ^{31}P SSNMMR spectrum (Figure 2d), the signals for $NaPF_6$ (–145 ppm) and the impurities (16 ppm) are well separated. Integration of the two signals gives a $NaPF_6$: impurity ratio of 1:0.0071, indicating a high purity sample. The ^{23}Na SSNMR spectrum has a single peak at –20.6 ppm, consistent with $NaPF_6$ (Figure 2c), with no evidence for NaF. Conversely, multinuclear SSNMR spectra recorded on a commercial sample of $NaPF_6$ showed the presence of impurities; tentatively assigned to $NaHF_2$ (Figures S2.2.5–S2.2.7).

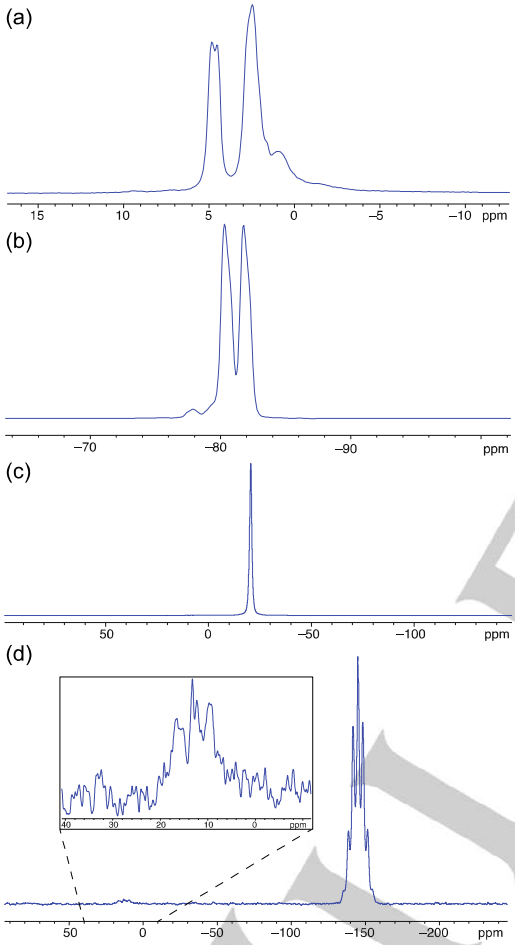

Figure 2. (a) ^{1}H, (b) ^{19}F, (c) ^{23}Na, and (d) ^{31}P solid-state NMR spectra of synthesized $NaPF_6$. The inset in panel (d) shows an expanded view with the signal of the hydrolysis products visible.

As the level of hydrolysis and degradation products present in the $NaPF_6$ salt affects the electrolyte concentration that can be achieved, we looked to determine the concentration range that could be produced from our high purity $NaPF_6$ salt in a binary mixture of ethylene carbonate: diethyl carbonate (EC:DEC 1:1 v/v) solvent. A 1 M solution could easily be obtained with minimal stirring at room temperature, giving a transparent electrolyte solution within minutes. A similar story was found when making a 2 M solution, however upon increasing the concentration to 3 M more vigorous stirring for 30 mins was required to obtain a clear solution. Saturation of the solution occurs at higher concentration, with the 3.5 M concentration electrolyte having very high viscosity and gel-like appearance, as well as containing undissolved $NaPF_6$. The electrolyte solutions become pale yellow in colour and less transparent as the concentration increases beyond 1 M (Figure S4.1.1).

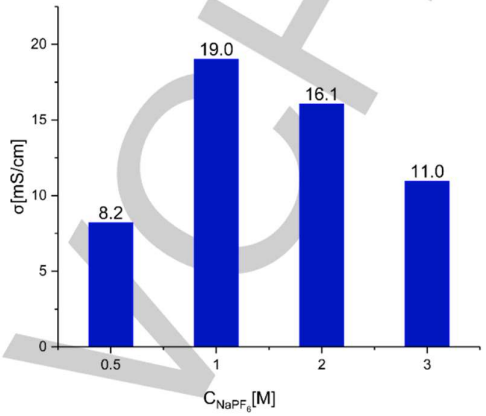

Figure 3. Electrolyte conductivity vs. concentration of $NaPF_6$ electrolytes. Measured in RHD instruments TSC 1600 Closed conductivity cell, the cell constant (K) is 13 cm^{-1} at T = 35 °C using impedance spectroscopy 1MHz–1Hz 10 mV amplitude.

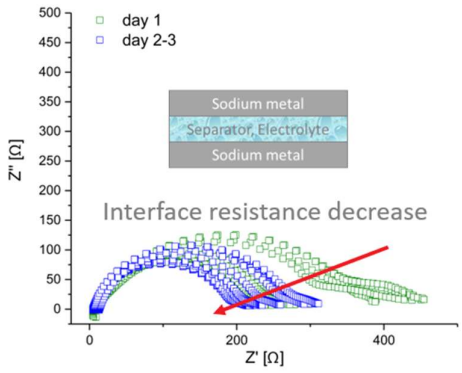

Figure 4. Impedance for 2 M $NaPF_6$ electrolyte (EC:DEC 1:1 v/v) from Na metal symmetric cell in coin cell.

The absence of insoluble impurities in our synthesized $NaPF_6$ allows for the accurate study of ultra-concentrated electrolytes, with the maximum electrolyte conductivity obtained with 1 M electrolyte solution (19.0 mS/cm at T = 35 °C), larger than the conductivity values of 8.2, 16.1 and 11.0 mS/cm for 0.5 M, 2.0 M and 3.0 M electrolyte solutions, respectively (Figure 3). Electrolyte conductivity and the aging of the native solid-electrolyte interphase (SEI) were then measured in Na-Na symmetric cells in the concentration range 1–3 M using electrochemical impedance spectroscopy (EIS) measurements between 1 MHz and 0.1 Hz (Figures 4 and S3.4–3.6). Consecutive impedance spectra were recorded for 70 hours after cell assembly and Nyquist plots accumulated during the first 70 hours from cell assembly are shown in Figure 4. It is assumed that the main contribution to the low-frequency conductivity is the sodium SEI, thus the evolution of the low-frequency conductivity is attributed to the aging, reorganization and dissolution of the SEI

during rest (Figure S3.7). The interface impedance for the ultra-concentrated (>2 M) electrolytes is around 300 Ω (6.3 µS/cm), while for 1 M it is around 500 Ω (3.8 µS/cm) at the same storage time. More importantly, the interface stabilization is slower for the 1 M electrolyte (Figures 4, S3.6), which could be the result of different SEI compositions, structures, or dissolution rate.

The electrochemical stability window (ESW) of our synthesized $NaPF_6$ electrolyte was determined using cyclic voltammetry (CV). Mixtures of 1–3 M $NaPF_6$ in EC:DEC (1:1 v/v) were tested in three-electrode cells using glassy carbon, stainless steel, and aluminium as working electrodes (WE); sodium metal was used as the counter and quasi-reference electrode (Figures 5, S3.1–S3.3). The current density of both oxidation (>4 V) and reduction (<1 V) waves decrease with the cycle number (Figure S3.1). The electrochemical stability of $NaPF_6$ vs. aluminium was investigated (Figure 5) and it was found that the measured current is three times lower for 2 M and 3 M electrolytes, in turn showing that the electrolyte electrochemical stability towards the current collectors is noticeably affected by the concentration of $NaPF_6$

.

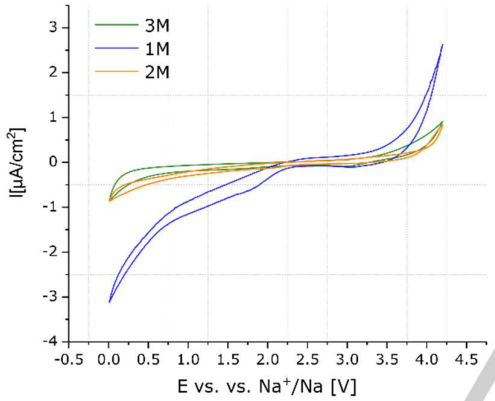

Figure 5. Cyclic voltammetry of 1–3 M $NaPF_6$ (EC:DEC 1:1 v/v) in three-electrode cell (WE - aluminium, CE- sodium metal, RE- sodium metal). 3rd cycle, measured at 1 mV/sec between 0.01 to 4.2 V.

The onset oxidation potential on glassy carbon, 304 stainless steel and aluminium for 1–3 M electrolyte solutions was observed at 3.7 V vs. sodium metal (Figures 5 and S3.1–3.3). However, EC oxidation onset potential above 5 V vs. sodium was recorded in the literature.[29–31] Traces of water in the electrolyte could be a possible cause for lower oxidation potentials.[32–34] While in the case of lithium, lithium hydroxide, which is generated by water reduction on the anode, tends to precipitate and accumulate in the SEI, sodium hydroxide remains in solution due to its high solubility (similarly to other sodium-SEI components).[35] This higher solubility results in less electrode passivation in sodium electrolytes and thus a larger water reduction current at lower potentials. Additionally, a minor reduction peak was observed at 1 V vs. sodium on the 1st cycle (Figures 5, S3.1, S3.3) and disappeared on the 3rd cycle (Figure S3.1). The most probable reaction responsible for this peak is the reduction of water, resulting in hydroxide formation and hydrogen evolution, consistent with the above proposals. The cathodic wave that starts around 0.6 V and peaks at 0.2–0.3 V is attributed to SEI formation.

Comparing the different electrolyte concentrations, 2 M and 3 M solutions of $NaPF_6$ were found to be more stable versus aluminium current collectors as opposed to 1 M $NaPF_6$ electrolyte. Moreover, the 2 M and 3 M electrolyte solutions resulted in lower impedance of the SEI on sodium compared to the impedance of the SEI in 1 M electrolyte which increased with time. This trend indicates a change in the break down and repair mechanism of the SEI and possibly lower SEI solubility with the increase in $NaPF_6$ concertation. However, since the bulk conductivity of the 2 M and 3 M electrolytes is lower compared to 1 M electrolytes, the choice of electrolyte concentration presents a potential trade-off between SEI and current collector stability, and cell power capability (further discussed in SI, S7).

Lastly, in order to showcase the high-grade nature of our synthesized $NaPF_6$, commercial 2- and 3-electrode pouch cells were produced independently by Faradion Limited, UK. 1 M electrolyte solutions of both our synthesized $NaPF_6$ and commercial Faradion baseline $NaPF_6$ were prepared in an ethylene carbonate, diethyl carbonate and propylene carbonate mixture (with no additives); the anode active material was a commercially available hard carbon and the cathode active material was sourced from Haldor-Topsoe A/S, synthesized according to Faradion's specification for a mixed phase O3/P2 layered oxide.[36,37] For the 3-electrode cell testing the reference electrode comprised an appropriately positioned tab of Na metal on aluminium. The results of these 3- and 2-electrode sodium-ion pouch cells showed comparable gravimetric capacity, rate capability and cycle life between our synthesized and Faradion baseline $NaPF_6$ electrolytes. In turn this shows that our $NaPF_6$ salt is compatible and stable electrochemically with both anode and cathode (Figure 6 and SI). Lastly, these results confirm the quality is as good as the commercial baseline electrolyte and the $NaPF_6$ produced is suitable for battery use.

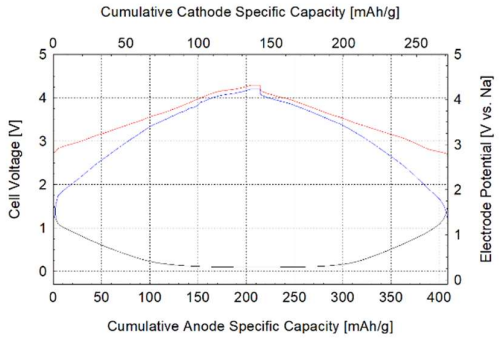

Figure 6. Cell voltage (V) and Anode and Cathode (V vs. Na) vs. cumulative active material specific capacity. Collected from 2nd cycle at an approximate constant current rate of C/7 for charge and discharge using cell voltage limits of 1.0 and 4.2 V. The cell voltage trace is in blue, the cathode voltage profile versus a Na metal reference electrode in red and the anode voltage profile in black. Electrolyte is our synthesized $NaPF_6$ (described above).

In conclusion this work demonstrates a simple, low cost and scalable synthetic route for producing high-grade $NaPF_6$ that is as pure as the highest-grade battery electrolyte available, and has identical electrochemical performance at 1 M concentration, as demonstrated in commercial 2- and 3-electrode pouch cells by Faradion. Our protocol avoids the use of HF or aqueous conditions and the absence of insoluble impurities such as NaF means that a 1 M concentration solution can easily be achieved and up to 3 M solutions can be prepared accurately in standard electrochemical solvents. Importantly, electrochemical

measurements reveal potential benefits of using higher concentration electrolyte solutions on SEI characteristics, which may be of value in the optimization of battery performance and lifetime.

Acknowledgements

The authors would like to acknowledge the Faraday Institution FIRG018 Next Generation Na-ion Batteries for funding.

Keywords: Battery • Electrolyte • NMR • Sodium-ion batteries • SEI

[1] N. Yabuuchi, K. Kubota, M. Dahbi, S. Komaba, *Chem. Rev.*, **2014**, *114*, 11636–11682.
[2] X. Pu, H. Wang, D. Zhao, H. Yang, X. Ai, S. Cao, Z. Chen, Y. Cao, *Small*, **2019**, *15*, 1805427.
[3] P. K. Nayak, L. Yang, W. Brehm, P. Adelhelm, *Angew. Chem. Int. Ed.*, **2018**, *57*, 102–120.
[4] T. Perveen, M. Siddiq, N. Shahzad, R. Ihsan, A. Ahmad, M. I. Shahzad, *Renew. Sustain. Energy Rev.*, **2020**, *119*, 109549.
[5] D. Kundu, E. Talaie, V. Duffort, L. F. Nazar, *Angew. Chem. Int. Ed.*, **2015**, *54*, 3431–3448.
[6] C. Vaalma, D. Buchholz, M. Weil, S. Passerini, *Nat. Rev. Mater.*, **2018**, *3*, 18013.
[7] T. Kim, W. Song, D.-Y. Son, L. K. Ono, Y. Qi, *J. Mater. Chem. A*, **2019**, *7*, 2942–2964.
[8] A. Ponrouch, D. Monti, A. Boschin, B. Steen, P. Johansson, M. R. Palacín, *J. Mater. Chem. A*, **2015**, *3*, 22–42.
[9] Z. Lin, Q. Xia, W. Wang, W. Li, S. Chou, *InfoMat*, **2019**, *1*, 376–389.
[10] G. G. Eshetu, G. A. Elia, M. Armand, M. Forsyth, S. Komaba, T. Rojo, S. Passerini, *Adv. Energy Mater.*, **2020**, *10*, 2000093.
[11] C. Bommier, X. Ji, *Small*, **2018**, *14*, 1703576.
[12] H. Che, S. Chen, Y. Xie, H. Wang, K. Amine, X.-Z. Liao, Z.-F. Ma, *Energy Environ. Sci.*, **2017**, *10*, 1075–11011.
[13] A. Ponrouch, E. Marchante, M. Courty, J.-M. Tarascon, M. R. Palacín, *Energy Environ. Sci.*, **2012**, *5*, 8572–8583.
[14] L. A. Ma, A. J. Naylor, L. Nyholm, R. Younesi, *Angew. Chem. Int. Ed.*, **2021**, *60*, 4855–4863.
[15] P. Barnes, K. Smith, R. Parrish, C. Jones, P. Skinner, E. Storch, Q. White, C. Deng, D. Karsann, M. L. Lau, J. J. Dumais, E. J. Dufek, H. Xiong, *J. Power Sources*, **2020**, *447*, 227363.
[16] L. Terborg, S. Nowak, S. Passerini, M. Winter, U. Karst, P. R. Haddad, P. N. Nesterenko, *Anal. Chim. Acta*, **2012**, *714*, 121–126.
[17] A. Bhide, J. Hofmann, A. K. Dürr, J. Janek, P. Adelhelm, *Phys. Chem. Chem. Phys.*, **2014**, *16*, 1987–1998.
[18] M. M. Woyski, W. J. Shenk, E. R. Pellon, *Inorganic Syntheses*, **1950**, *3*, 111–117.
[19] A. F. Clifford, A. G. Morris, *J. Inorg. Nucl. Chem.*, **1957**, *5*, 71–75.
[20] M. D. S. Lekgoathi, J. P. Le Roux, WO 2015/150862 A1, **2015**.
[21] J.-R. Hamon, D. Astruc, *J. Am. Chem. Soc.*, **1983**, *105*, 5951–5952.
[22] R. Younesi, G. M. Veith, P. Johansson, K. Edström, T. Vegge, *Energy Environ. Sci.*, **2015**, *8*, 1905–1922.
[23] *Fluorinated Materials for Energy Conversion*, eds. T. Nakajima, H. Groult, Elsevier, 1st edn, 2005.
[24] R. D. W. Kemmitt, D. R. Russell, D. W. A. Sharp, *J. Chem. Soc.*, **1963**, 4408–4413.
[25] R. A. Wiesboeck., *US Pat.*, 3654330, **1972**.
[26] J.-H. Kim, K. Nagahara, S. Yonezawa, M. Takashima, *Chem. Lett.*, **2004**, *33*, 884–885.
[27] E. N. Keyzer, H. F. J. Glass, Z. Liu, P. M. Bayley, S. E. Dutton, C. P. Grey, D. S. Wright, *J. Am. Chem. Soc.*, **2016**, *138*, 8682–8685.
[28] D. Barr, R. Snaith, D. S. Wright, R. E. Mulvey, K. Wade, *J. Am. Chem. Soc.*, **1987**, *109*, 7891–7893.
[29] L. T. M. Le, T. D. Vo, K. H. P. Ngo, S. Okada, F. Alloin, A. Garg, P. M. L. Le, *J. Mol. Liq.*, **2018**, *271*, 769–777.
[30] B. L. D. Rinkel, D. S. Hall, I. Temprano, C. P. Grey, *J. Am. Chem. Soc.*, **2020**, *142*, 15058–15074.
[31] M. L. P. Le, N. A. Tran, H. P. K. Ngo, T. G. Nguyen, V. M. Tran, *J. Solution Chem.*, **2015**, *44*, 2332–2343.
[32] N. Dubouis, A. Serva, E. Salager, M. Deschamps, M. Salanne, A. Grimaud, *J. Phys. Chem. Lett.*, **2018**, *9*, 6683–6688.
[33] C. Cometto, G. Yan, S. Mariyappan, J.-M. Tarascon, *J. Electrochem. Soc.*, **2019**, *166*, A3723–A3730.
[34] M. Metzger, B. Strehle, S. Solchenbach, H. A. Gasteiger, *J. Electrochem. Soc.*, **2016**, *163*, A1219–A1225.
[35] D. Aurbach, M. Daroux, P. Faguy, E. Yeager, *J. Electroanal. Chem.*, **1991**, *297*, 225–244.
[36] J. Barker, R. Heap, WO Application, 2019197812, **2020** (priority date April 9, 2018).
[37] R. Sayers, J. Barker, R. Heap, US Patent 10550007, **2020** (priority date May 22, 2014).

Entry for the Table of Contents

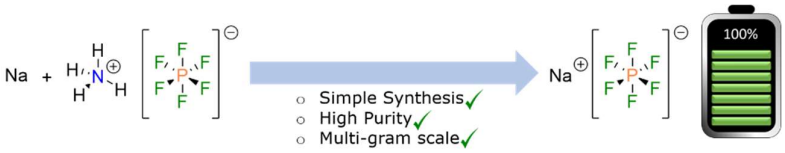

This work addresses the urgent need to produce high grade sodium hexafluorophosphate electrolyte salt for sodium-ion batteries. Our synthesis involves the addition of ammonium hexafluorophosphate to sodium metal under anhydrous conditions, which prevents the formation of NaF and other commonly found hydrolysis products seen in commercial samples. The high purity allows for up to 3 M electrolyte concentrations to be achieved.

Institute and/or researcher Twitter usernames: @darren_ould, @SvetlanaMenkin, @ChemCambridge @GreyGroupCam

WILEY-VCH